Investigation of the Alkali-Metal Vanadium Oxide Xerogel Bronzes: $A_xV_2O_5{\cdot}nH_2O$ (A = K and Cs)

Y.-J. Liu,[†,§] J. A. Cowen,[‡,§] T. A. Kaplan,[‡,§] D. C. DeGroot,[⊥] J. Schindler,[⊥] C. R. Kannewurf,[⊥] and M. G. Kanatzidis*[,†,§]

Department of Chemistry, Michigan State University, East Lansing, Michigan 48824; Department of Physics, Michigan State University, East Lansing, Michigan 48824; Center for Fundamental Materials Research, Michigan State University, East Lansing, Michigan 48824; and Department of Electrical Engineering and Computer Science, Northwestern University, Evanston, Illinois 60208

Received January 18, 1995. Revised Manuscript Received June 13, 1995[⊗]

The synthesis of bronze-like $A_xV_2O_5{\cdot}nH_2O$ xerogels (A = K and Cs, $0.05 < x < 0.6$) and systematic characterization of their chemical, structural, spectroscopic magnetic, and charge-transport properties are reported. These materials were prepared by the reaction of $V_2O_5{\cdot}nH_2O$ with various amounts of alkali iodide (KI and CSI) in acetone under N_2 atmosphere for 3 days. X-ray diffraction and spectroscopic data indicate that the V_2O_5 framework in $A_xV_2O_5{\cdot}nH_2O$ maintains the pristine V_2O_5 xerogel structure. The increased V^{4+} (d^1) concentration in the V_2O_5 framework causes the disappearance of EPR hyperfine structure and the increase of magnetic susceptibility and electrical conductivity. The optical diffuse reflectance spectra of these compounds show characteristic absorption bands due to inter-valence (V^{4+}/V^{5+}) charge-transfer transitions. The magnetic behavior is best described as Curie–Weiss type coupled with temperature-independent paramagnetism (TIP). The Curie constant and EPR peak width of the $A_xV_2O_5{\cdot}nH_2O$ materials show unusual behavior consistent with strong antiferromagnetic coupling of neighboring V^{4+} centers. The electrical conductivity slightly increases with V^{4+} concentration, and its temperature dependence indicates a thermally activated process. The thermoelectric power of the $A_xV_2O_5{\cdot}nH_2O$ materials is negative and becomes less negative with increasing V^{4+} concentration (i.e., increasing x).

Introduction

Recently, we showed that the redox intercalation of organic monomers such as aniline, pyrrole, and 2,2′-bithiophene yields layered materials containing monolayers of conductive polymers in the intralamellar space of V_2O_5 xerogel.[1] The vanadium oxide network is reduced to form V^{4+} centers while organic monomers are oxidatively polymerized into electrically conductive polymers. This results in new molecular composites of two electrically active but chemically diverse components: organic conductive polymers and inorganic vanadium bronzes. To achieve a better understanding of the role of the conductive polymer inside the oxide sheets and its influence on the properties of the molecular composites, it is important to understand the nature and properties of the reduced V_2O_5 framework alone. For this we need a material with the same reduced V_2O_5 structure but intercalated with simple chemical species that would not interfere with a physicochemical study of the oxide framework. Of course, numerous studies have been published on *crystalline* bronze phases of the type $A_xV_2O_5$[2], but in these materials the V_2O_5 structure is different from that of V_2O_5 xerogels and it varies with A and x. Therefore, these materials are not representative of the xerogel bronzes. To our knowledge, complete and systematic studies of compounds with a reduced V_2O_5 xerogel framework have not been reported.[3] A series of reduced V_2O_5 xerogels was prepared in this work by the reaction of the xerogel with various amounts of alkali iodide (KI and CsI). The intercalants, K^+ and Cs^+, are closed-shell ions which can be considered as "innocent" species (e.g., diamagnetic and insulating), thus allowing the study of the properties of the reduced V_2O_5 framework with no interference from the guests. The structure of the vanadium oxide framework remains the same in this case regardless of the identity of the alkali ion or its concentration (at least for x values <0.5). In this paper, we report the synthesis of a series of bronze-like V_2O_5 xerogels, namely $A_xV_2O_5{\cdot}nH_2O$, and their X-ray diffraction, optical, infrared, and spin resonance spectroscopic, magnetic, and charge-transport characterization as a function of x (i.e., V^{4+} concentration). The Curie constant and EPR peak width of the $A_xV_2O_5{\cdot}nH_2O$ materials show unusual behavior, namely, nonlinear variation with x; in particular there is a maximum value at $x \sim 0.3$, suggesting strong antiferromagnetic coupling of V^{4+} centers.

[†] Department of Chemistry.
[‡] Department of Physics.
[§] Center for Fundamental Materials Research.
[⊥] Department of Electrical Engineering and Computer Science.
[⊗] Abstract published in *Advance ACS Abstracts,* July 15, 1995.

(1) (a) Kanatzidis, M. G.; Wu, C.-G.; Marcy, H. O.; Kannewurf, C. R. *J. Am. Chem. Soc.* **1989**, *111*, 4139–4141. (b) Wu, C-G.; Kanatzidis, M. G.; Marcy, H. O.; DeGroot, D. C.; Kannewurf, C. R. *Polym. Mater. Sci. Eng.* **1989**, *61*, 969–973. (c) Kanatzidis, M. G.; Wu, C.-G.; Marcy, H. O.; DeGroot, D. C.; Kannewurf, C. R. *Chem. Mater.* **1990**, *2(3)*, 222–224.

(2) (a) Murphy, D. W.; Christian, P. A.; DiSalvo, F. J.; Waszczak, J. V. *Inorg. Chem.* **1979**, *18(10)*, 2800–2803. (b) Chakraverty, B. K.; Sienko, M. J. *Phys. Rev. B* **1978**, *17(10)*, 3781–3789. (c) Gendell, J.; Cotts, R. M.; Sienko, M. J. *J. Chem. Phys.* **1962**, *37(2)*, 220–225.

(3) (a) Babonneau, F.; Barboux, P.; Josien, F. A.; Livage, J. *J. Chim. Phys.* **1985**, *82*, 761–766. (b) Bullot, J.; Cordier, P.; Gallais, O.; Gauthier, M.; Babonneau, F. *J. Non-Cryst. Solids* **1984**, *68*, 135–146.

0897-4756/95/2807-1616$09.00/0

Experimental Section

Materials. Sodium metavanadate ($NaVO_3$), potassium iodide (KI), and cesium iodide (CsI) were purchased from Aldrich Co., Milwaukee, WI, and were used without further purification. Elemental analyses were done by Galbraith Laboratories, Knoxville, TN, and Oneida Research Services, Inc., Whitesboro, NY.

Measurements. Infrared spectra were recorded from 4000 to 400 cm^{-1} with a resolution of 1 cm^{-1} on a Nicolet 740 FT-IR spectrometer. Samples were recorded in a pressed KBr matrix under N_2 flow. IR diffuse reflectance spectra were also recorded on the same instrument equipped with a reflectance attachment purchased from Spectra Tech. Inc. Samples were pressed into pellets and directly put on a sample holder. A gold mirror was used as the reference.

X-ray diffraction was carried out on a Rigaku rotating anode X-ray powder diffractometer, Rigaku-Denki/RW400F2 (Rotaflex), at 45 kV and 100 mA with a scintillation counter detector and a graphite monochromator to yield Cu Kα (wavelength 1.541 84 Å) radiation. Data were collected at room temperature over the range $2° \leq 2\theta \leq 80°$ in increments of 0.01°.

Electron paramagnetic resonance (EPR) spectra were obtained using a Varian E-4 spectrometer operating at 9.5 GHz (X band) and at room temperature. Solid samples were scanned from 2700 to 3700 G at 8 G field modulation and 0.03 s time constant. The g value was obtained with reference to the standard diphenylpicrylhydrazine (DPPH).

Magnetic susceptibility measurements were done on a MPMS Quantum Design SQUID system (superconducting quantum interference device) with a magnetic field of 5000 G. A known quantity of sample was placed in a plastic bag and purged with Ar gas. Data were collected with an ascending ramp from 5 to 300 K and then corrected for the diamagnetic components using values obtained from the literature.[4]

Direct-current electrical conductivity and thermopower measurements were performed in the usual four-probe geometry with 60 and 25 mm gold wires used for the current and voltage electrodes, respectively.[5] Thermoelectric power measurements were made by using a slow ac technique with 60 mm gold wires serving to support and conduct heat to the sample, as well as to measure the voltage across the sample resulting from the applied temperature gradient.[6]

Optical diffuse reflectance spectra were measured at room temperature with a Shimadzu UV-3101PC double-beam, double-monochromator spectrophotometer. The composite films were placed above $BaSO_4$ on a sample holder. $BaSO_4$ powder was used as a reference. The absorption spectrum was calculated from the reflectance data using the Kubelka–Munk function: $\alpha/S = (1 - R)^2/2R$. R is the reflectance, α is the absorption coefficient, and S is the scattering coefficient which is practically wavelength independent when the particle size is larger than 5 μm.[7]

Quantitative elemental analysis was done by the SEM/EDS (scanning electron microscopy/energy-dispersive spectroscopy) technique on a JEOL JSM-35C microscope equipped with a Tracor Northern TN 55000 X-ray microanalysis attachment. Samples were glued on an aluminum stub with conductive carbon paint for the dissipation of accumulated charges. Typical experimental conditions are as follows: accelerating voltage, 20 keV; detector window, beryllium; takeoff angle, 27°; accumulation time, 60 s. A standardless quantitative analysis software program was used to analyze the characteristic X-ray peaks of the elements present in the sample. Correction factors for K/V and Cs/V ratios were determined from known compounds such as KVO_3 and $CsVO_3$. The alkali-to-vanadium ratios for each sample were obtained by averaging three measurements.

The calculation of a one-dimensional (1-D) electron density map was based on the X-ray reflection data using the observed ($00l$) group of reflections. The data were obtained from a film of $Cs_{0.27}V_2O_5{\cdot}nH_2O$. Eight reflections were used out to d_{008} = 1.37 Å. The intensities were obtained from the integrated peak areas. The structure factors of these reflections were derived from their intensities and corrected for Lorentz–polarization effects. The signs of the phases for the structure factor calculation were obtained directly from the scattering contributions of the V_2O_5 framework alone. The signs of the phases were also checked by recalculation including the contribution of the Cs^+ ions. All but one reflection changed sign which did not significantly change the electron density pattern.

Preparation of V_2O_5 Xerogel. V_2O_5 xerogel was prepared by a reported method.[8] Sodium metavanadate (4 g, 32.8 mmol) was dissolved in 250 mL of distilled water. The resulting solution was eluted through a column packed with H^+ ion-exchange resin (Dowex-50X2-100) forming a pale-orange solution of HVO_3. Upon standing, this solution polymerized to a red V_2O_5 gel in several days. The gel was then poured on flat substrates and the excess water was slowly evaporated to yield the V_2O_5 xerogel as a thick dark red film. The definition of a zerogel is product remaining after solvent evaporation from a gel.

Preparation of $A_xV_2O_5{\cdot}nH_2O$. Powdered V_2O_5 xerogel (0.5 g, 3.38 mmol) was added to a 50 mL of acetone with the stoichiometric amount of KI or CsI. The KI/V_2O_5 and CsI/V_2O_5 molar ratios were varied from 0.1 to 1.0 in increments of 0.1. The reaction was stirred under N_2 atmosphere for 3 days. The dark product was filtered, washed with acetonitrile, and then dried under vacuum. The compositions of $A_xV_2O_5{\cdot}nH_2O$ compounds were determined from elemental analysis and SEM/EDS. An attempt to produce the $A_xV_2O_5{\cdot}nH_2O$ materials with $x > 0.6$ failed, yielding amorphous products. The value of n is ~1.1 when $0.05 < x < 0.1$ and ~0.5–0.6 when $x > 0.1$.

Results and Discussion

Synthesis and Spectroscopy. The reduced V_2O_5 xerogels were produced according to

$$yAI + V_2O_5{\cdot}nH_2O \rightarrow A_yV_2O_5{\cdot}nH_2O + (y/2)I_2 \quad (1)$$
$$A = K, Cs$$

This intercalation method was used earlier to insert alkali ions into orthorhombic V_2O_5.[2a] The V_2O_5 xerogel oxidizes iodide to iodine and the alkali ions are intercalated into the reduced framework to achieve electroneutrality. The composition, interlayer distance, and infrared spectroscopic data for $K_xV_2O_5{\cdot}nH_2O$ and $Cs_xV_2O_5{\cdot}nH_2O$ compounds are summarized in Table 1. The $A_xV_2O_5{\cdot}nH_2O$ compounds are brown or green when $x < 0.1$ and blue when $x \geq 0.1$. The amount of hydrated water decreases with increasing x from a value of 1.8 when $x = 0$ (V_2O_5 xerogel) to ~0.6 when $x > 0.1$.[9] Generally, the infrared spectra of the $A_xV_2O_5{\cdot}nH_2O$ are similar and show three characteristic vibration bands from the V_2O_5 framework below 1100 cm^{-1}. A typical infrared spectrum from $K_{0.33}V_2O_5{\cdot}nH_2O$ is shown in Figure 1. The band at ~1000 cm^{-1} is assigned to the V=O stretching vibration and the bands at ~750 and ~500 cm^{-1} are attributed to the in-plane and out-of-

(4) Boudreaux, E. A.; Mulay, L. N. *Theory and Applications of Molecular Paramagnetism;* John Wiley & Sons: New York, 1976.
(5) Lyding, J. W.; Marcy, H. O.; Marks, T. J.; Kannewurf, C. R. *IEEE Trans. Instrum. Meas.* **1988**, *37*, 76–80.
(6) Marcy, H. O.; Marks, T. J.; Kannewurf, C. R. *IEEE Trans. Instrum. Meas.* **1990**, *39*, 756–760.
(7) (a) Wendlandt, W. W.; Hecht, H. G. *Reflectance Spectroscopy;* Interscience Publishers: New York, 1966. (b) Kotüm, G. *Reflectance Spectroscopy;* Springer-Verlag: New York, 1969. (c) Tandon, S. P.; Gupta, J. P. *Phys. Status Solidi* **1970**, *38*, 363–367.
(8) Lemerle, J.; Nejem, L.; Lefebvre, J. *J. Inorg. Nucl. Chem.* **1980**, *42*, 17–20.
(9) This was determined from thermal gravimetric analysis (TGA) experiments.

Table 1. Summary of Composition, Color, Interlayer Spacing, and Infrared Data for $K_xV_2O_5{\cdot}nH_2O$ and for $Cs_xV_2O_5{\cdot}nH_2O$[a]

formula	color	*d* spacing (Å)	vibration bands (cm^{-1})
$V_2O_5{\cdot}1.8H_2O$	red	11.55	1015, 760, 510
$K_{0.08}V_2O_5{\cdot}1.1H_2O$	green	11.65	1012, 759, 513
$K_{0.26}V_2O_5{\cdot}nH_2O$	dark blue	10.28	999, 762, 527
$K_{0.33}V_2O_5{\cdot}nH_2O$	dark blue	10.10	996, 766, 537
$K_{0.39}V_2O_5{\cdot}nH_2O$	dark blue	10.05	994, 760, 522
$K_{0.44}V_2O_5{\cdot}nH_2O$	dark blue	9.87	996, 774, 547
$K_{0.47}V_2O_5{\cdot}nH_2O$	dark blue	9.86	996, 761, 530
$K_{0.56}V_2O_5{\cdot}nH_2O$	dark blue	9.72	984, 759, 527
$Cs_{0.07}V_2O_5{\cdot}1.1H_2O$	brown	11.65	1012, 756, 513
$Cs_{0.18}V_2O_5{\cdot}nH_2O$	dark blue	11.2	1010, 760, 520
$Cs_{0.26}V_2O_5{\cdot}nH_2O$	dark blue	10.8	1006, 762, 532
$Cs_{0.28}V_2O_5{\cdot}nH_2O$	dark blue	10.8	999, 754, 535
$Cs_{0.35}V_2O_5{\cdot}nH_2O$	dark blue	10.8	999, 755, 524
$Cs_{0.38}V_2O_5{\cdot}nH_2O$	dark blue	10.8	997, 762, 530
$Cs_{0.41}V_2O_5{\cdot}nH_2O$	dark blue	10.7	994, 755, 523

[a] *n* is in the range 0.5–0.6.

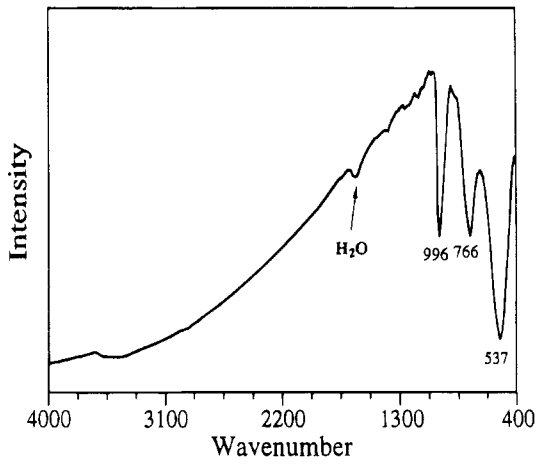

Figure 1. Infrared spectrum of $K_{0.33}V_2O_5{\cdot}0.5H_2O$ (KBr pellet).

plane V–O–V vibrations,[10] respectively. The presence of the three bands suggests that the reduced V_2O_5 framework is structurally intact with respect to the pristine $V_2O_5{\cdot}nH_2O$ framework. The V=O stretching vibration generally shifts to lower energy as the alkali ion concentration increases; see Figure 2. The red shift is due to the addition of electrons into antibonding d orbitals of vanadium, probably coupled with the ionic interactions between the oxygen of V=O and the intercalated alkali ions.

The optical absorption spectra of the $A_xV_2O_5{\cdot}nH_2O$ compounds show a very broad band, centered around 1400 nm with tails extending into both the infrared and visible region; see Figure 3. The band, which is described as an intervalence electronic transition from V^{4+} to V^{5+} centers,[3] is absent in pristine V_2O_5 xerogel due to the very small number of V^{4+} centers. The appearance of this intense intervalence band confirms that the V_2O_5 framework is reduced. Interestingly, these materials show additional electronic absorption peaks in the infrared region of the spectrum, and this is relevant to the magnetic properties of these materials to be discussed later.

X-ray Diffraction Studies. The structure of the $V_2O_5{\cdot}nH_2O$ xerogel is not accurately known but two motifs have been proposed. Livage and co-workers

(10) Abello, L.; Husson, E.; Repelin, Y.; Lucazeau, G. *J. Solid State Chem.* **1985**, *56*, 379–389.

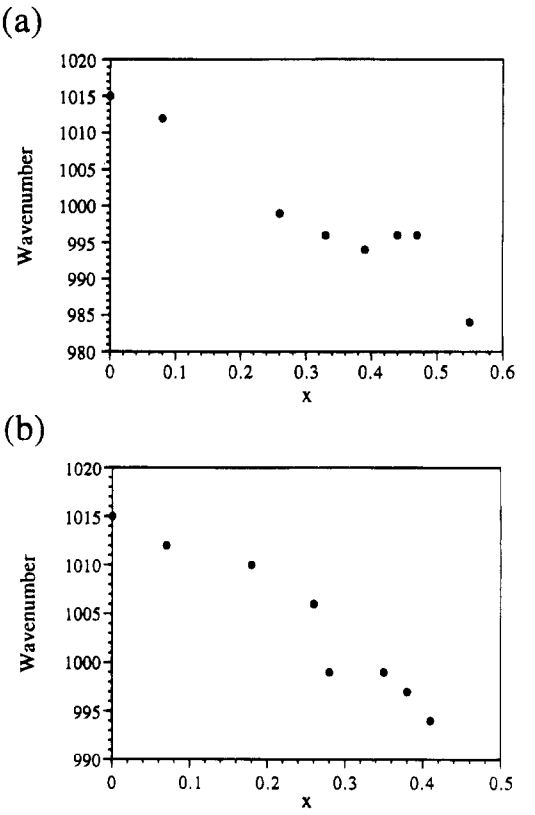

Figure 2. Spectral shifts of V=O vibration energy as a function of *x*: (a) $K_xV_2O_5{\cdot}nH_2O$ and (b) $Cs_xV_2O_5{\cdot}nH_2O$.

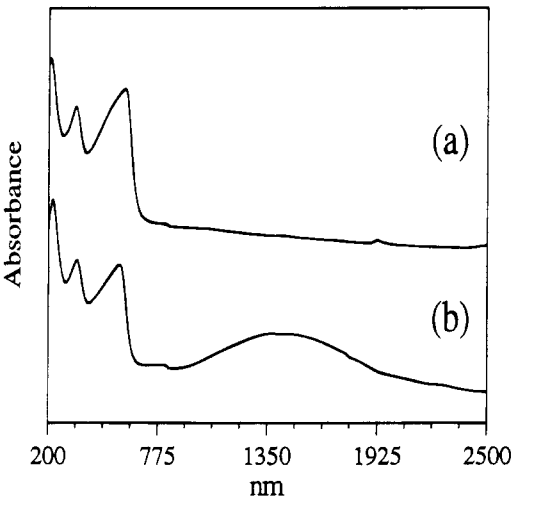

Figure 3. Optical absorption spectra of (a) V_2O_5 xerogel and (b) $Cs_{0.18}V_2O_5{\cdot}0.5H_2O$.

suggested a layered structure composed of a single corrugated slab of V_2O_5 with a corrugation step of 2.8 Å.[11] Between each corrugation step the layers have the same structure as crystalline V_2O_5. Oka and co-workers support a bilayer model with flat V_2O_5 slabs based on the structure of $Na_xV_2O_5$.[12] In the Oka model two flat V_2O_5 slabs face each other at a distance of 2.8 Å. The two proposed models, shown in Figure 4, mostly satisfy the observed X-ray diffraction data in the reflection

(11) (a) Legendre, J.-J.; Aldebert, P.; Baffier, N.; Livage, J. *J. Colloid Interface Sci.* **1983**, *94(1)*, 84–89. (b) Livage, J. *Chem. Mater.* **1991**, *3*, 573–593.

(12) (a) Yao, T.; Oka, Y.; Yamamoto, N. *Mater. Res. Bull.* **1992**, *27*, 669–675. (b) Yao, T.; Oka, Y.; Yamamoto, N. *J. Mater. Chem.* **1992**, *2(3)*, 331–336. (c) Yao, T.; Oka, Y.; Yamamoto, N. *J. Mater. Chem.* **1992**, *2(3)*, 337–340.

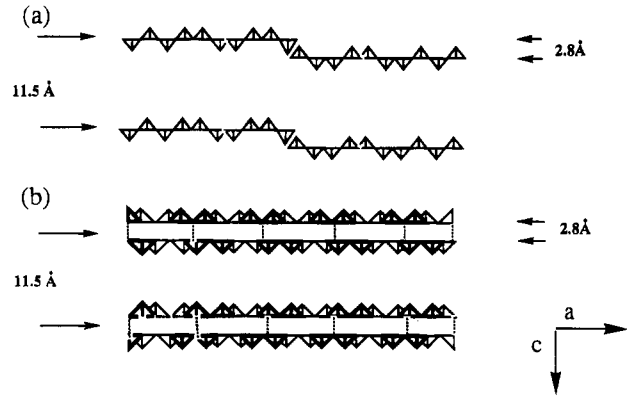

Figure 4. Schematic illustration of the structure of V_2O_5 xerogel projected onto the ac plane as proposed by (a) Livage et al.[9] and (b) Oka et al.[10] and (c) the structure of orthorhombic V_2O_5 projected in a plane perpendicular to the stacking axis.

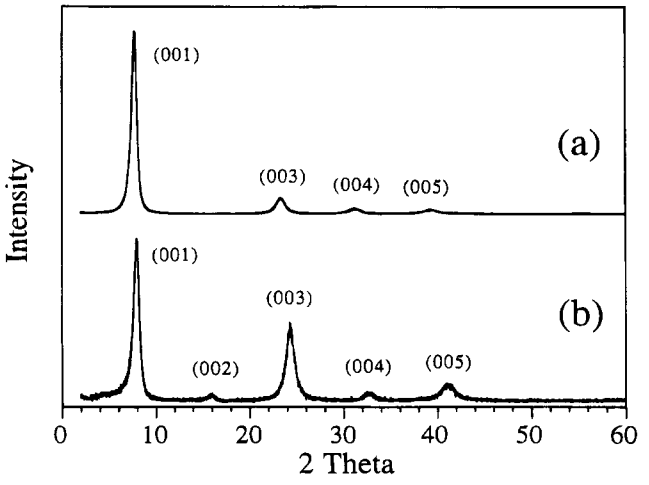

Figure 5. X-ray diffraction patterns of (a) V_2O_5 xerogel and (b) $Cs_{0.27}V_2O_5{\cdot}0.5H_2O$.

mode (i.e., the 00*l* class of reflections). Poor agreement between either model and the observed X-ray diffraction data is observed when the data are collected in the transmission mode (i.e., among the *hk*0 class of reflections). However, on the basis of the observed density of $V_2O_5{\cdot}nH_2O$ xerogel, which is ~2.5 g/cm^3, Oka's model appears to be most consistent (d_{calcd} ~2.87 g/cm^3). The Livage model gives a d_{calcd} ~ 1.5 g cm^{-3}. The densities of $A_xV_2O_5{\cdot}nH_2O$ range between 2.7 and 3.3 g/cm^3. Therefore, we prefer to use Oka's model.

The $A_xV_2O_5{\cdot}nH_2O$ materials were examined by X-ray diffraction. Figure 5 shows a typical X-ray diffraction pattern for the $A_xV_2O_5{\cdot}nH_2O$ compounds in which (00*l*) peaks dominate, indicating that the lamellar structure is maintained. The interlayer spacing decreases slightly from 11.65 Å when $x = 0.08$ to 9.72 Å when $x = 0.55$ in $K_xV_2O_5{\cdot}nH_2O$, and from 11.65 Å when $x = 0.07$ Å to 10.7 Å when $x = 0.41$ in $Cs_xV_2O_5{\cdot}nH_2O$ (Table 1). The decrease in the interlayer height with increasing x is due to the loss of intercalated water and the increased attractive interactions between the positively charged alkali ions and the negatively charged V_2O_5 layers. For the same x, the $Cs_xV_2O_5{\cdot}nH_2O$ show a slightly higher expansion than the $K_xV_2O_5{\cdot}nH_2O$, consistent with the larger size of Cs^+.

To determine the position of alkali ions in the V_2O_5 framework, we performed 1-D electron density calculations along the layer stacking direction (*c* axis) for

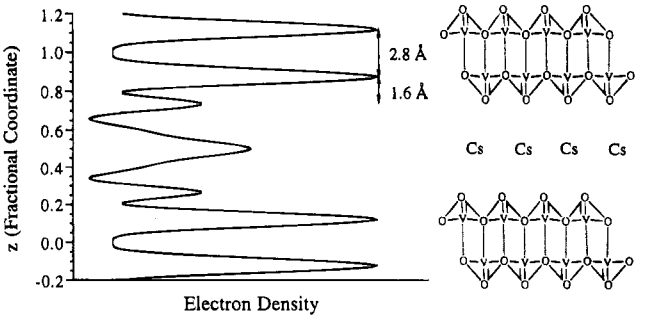

Figure 6. Projection of the electron density of $Cs_{0.27}V_2O_5{\cdot}nH_2O$ calculated from Oka's model. The strong peak at $z = 0.5$ is due to the projection of the Cs^+ ion.

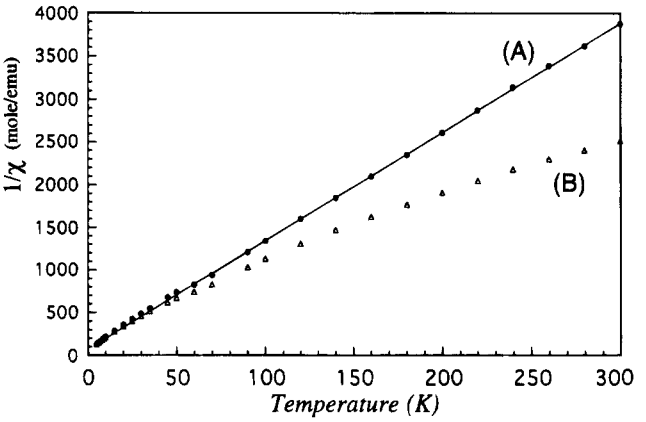

Figure 7. Inverse magnetic susceptibility as a function of temperature for $K_{0.47}V_2O_5{\cdot}nH_2O$: (a) $\chi_{(Curie-Weiss)}$ and (b) χ_m.

$Cs_{0.27}V_2O_5{\cdot}0.5H_2O$. The electron density function was phased, based on Oka's model, and the location of the Cs atom was determined from the projection of the calculated electron density on the *c* axis, as shown in Figure 6. The two strong peaks observed at $z = 0.87$ and 1.13 with a separation of 2.8 Å are due to the projection of the two different planes of vanadium atoms. The 2.8 Å distance corresponds to the separation of these two planes, or in the Livage model, to the corrugation step in each V_2O_5 slab. The peak at $z = 0.73$ corresponds to a distance of 1.6 Å from the vanadium planes and is consistent with vanadyl groups perpendicular to the layers. The peak at $z = 0.5$ is attributed to the projection of the Cs^+ ions; it reveals that they reside in a plane lying exactly in the middle of the interlayer gallery. Although this conclusion may seem intuitive, there are many examples in the literature where alkali atoms between layers lie on corrugated planes.[13] Similar conclusions can be extracted from calculations on other $A_xV_2O_5{\cdot}nH_2O$ compounds with $x < 0.3$. However, electron density calculations for the $A_xV_2O_5{\cdot}nH_2O$ with $x > 0.3$ were unreliable due to insufficient number of reflections.

Magnetic Susceptibility Studies. There are two novel aspects of the temperature dependent magnetic susceptibility of the $A_xV_2O_5{\cdot}nH_2O$ materials. First, the presence of a rather large temperature-independent paramagnetic (TIP) component which varies with x. We show in the following that this variation correlates with electronic absorptions which we have observed in the diffuse reflectance spectra (see below) and therefore can

(13) Park, Y.; DeGroot, D. C.; Schindler, J.; Kannewurf, C. R.; Kanatzidis, M. G. *Angew. Chem., Int. Ed. Engl.* **1991**, *30*, 1325–1328.

Table 2. Magnetic Susceptibility Data for $K_xV_2O_5{\cdot}nH_\infty O$ and $Cs_xV_2O_5{\cdot}nH_\infty O$ Compounds

x	χ_m[a] (emu/mol)	$\chi_{(TIP)}$ (emu/mol)	μ_{eff}[b] (spin only)	C	θ (K)
$K_{0.08}V_2O_5{\cdot}1.1H_\infty O$	2.67e−4	0.56 ± 4.0e−4	0.72 ± 0.07	0.06 ± 0.01	−2
$K_{0.26}V_2O_5{\cdot}nH_2O$	4.44e−4	1.1 ± 0.5e−4	0.89 ± 0.06	0.10 ± 0.01	−3.7
$K_{0.33}V_2O_5{\cdot}nH_2O$	5.30e−4	2.0 ± 0.5e−4	0.88 ± 0.07	0.11 ± 0.01	−5.7
$K_{0.39}V_2O_5{\cdot}nH_2O$	4.14e−4	1.4 ± 0.4e−4	0.83 ± 0.03	0.09 ± 0.01	−6
$K_{0.47}V_2O_5{\cdot}nH_\infty O$	3.98e−4	1.4 ± 0.4e−4	0.78 ± 0.06	0.08 ± 0.01	−7.8
$K_{0.55}V_2O_5{\cdot}nH_2O$	4.32e−4	1.7 ± 0.4e−4	0.78 ± 0.06	0.08 ± 0.01	−9.6
$Cs_{0.07}V_2O_5{\cdot}1.1H_2O$	2.13e−4	4.9 ± 2.0e−5	0.62 ± 0.04	0.05 ± 0.01	0.65
$Cs_{0.18}V_2O_5{\cdot}nH_2O$	3.83e−4	7.0 ± 4.0e−5	0.86 ± 0.06	0.09 ± 0.01	−1.6
$Cs_{0.26}V_2O_5{\cdot}nH_2O$	4.97e−4	1.4 ± 0.6e−4	0.89 ± 0.05	0.11 ± 0.02	−3.9
$Cs_{0.28}V_2O_5{\cdot}nH_2O$	5.75e−4	2.2 ± 0.5e−4	0.92 ± 0.06	0.10 ± 0.01	−5
$Cs_{0.35}V_2O_5{\cdot}nH_2O$	5.20e−4	1.9 ± 0.5e−4	0.88 ± 0.06	0.10 ± 0.01	−5
$Cs_{0.38}V_2O_5{\cdot}nH_2O$	5.14−e	2.0 ± 0.5e−4	0.86 ± 0.07	0.09 ± 0.01	−5.6
$Cs_{0.41}V_2O_5{\cdot}nH_2O$	5.38e−4	2.4 ± 0.5e−4	0.83 ± 0.10	0.09 ± 0.01	−7.2

[a] χ_m values at room temperature. [b] Calculated from $(\chi_m - \chi_{(TIP)})$.

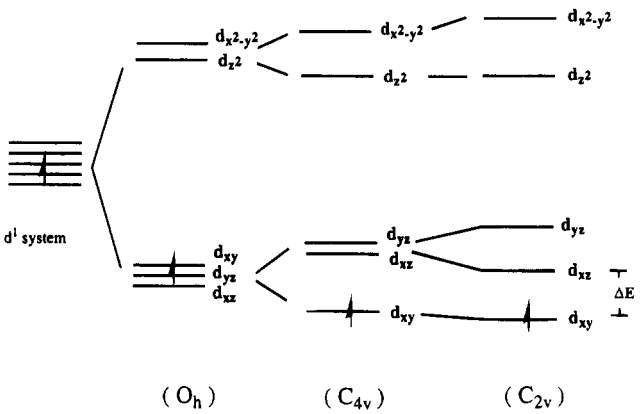

Figure 8. Simplified d orbital diagrams of V^{4+} in octahedral, square-pyramidal, and distorted square-pyramidal geometry. The latter geometry is most representative of the V^{4+} environment in the reduced V_2O_5 xerogel. (ΔE is the energy separation between d_{xz} and d_{xy} orbitals). The ordering of d_{xz}, d_{yz}, and d_{xy} levels depends on the extent of π acceptor character of d_{xz} and d_{yz} orbitals.

be attributed to van Vleck (TIP).[14] Second, the fact that the Curie constant C does not increase linearly with x as one expects from a simple Curie system but reaches a maximum at ~0.3 and then decreases. We have reproduced the general behavior of C with increasing x with a spin model which assumes that the nearest-neighbor V^{4+} ions are strongly coupled into antiferromagnetic dimers (see discussion below). Table 2 summarizes the susceptibility data for all compounds. The magnetic susceptibility data (see Figure 7) were fit to eq 2, the resulting $\chi_{(TIP)}$, C, and θ for the $A_xV_2O_5{\cdot}nH_2O$ compounds were extracted and are given in Table 2;

$$\chi_m = \frac{C}{T-\theta} + \chi_{(TIP)} \qquad (2)$$

where $C = Ng^2\beta^2/4k$ is the Curie constant for $S = 1/2$, and θ is the Weiss constant. N is the number of spins per mole, β is the bohr magneton of the electron, and k is Boltzman's constant. Depending on x, the μ_{eff} calculated from $C = (N_A\beta^2/3k)\mu_{eff}^2$ (N_A is Avogadro's number) is in the range between 0.6 and 1.0 μ_B, confirming the increased number of V^{4+} centers in the framework relative to pristine xerogel. The latter, which is the $x = 0$ member in the $A_xV_2O_5{\cdot}nH_2O$ series, has a μ_{eff} of ~0.3−0.4 μ_B because of residual V^{4+} impurities which unavoidably form during preparation. From the above expressions for C one finds that a μ_{eff} of ~0.35 μ_B corresponds to 0.04 unpaired spins per $V_2O_5{\cdot}nH_2O$.

The $\chi_{(TIP)}$ term originates from the second-order Zeeman effect which describes the interaction of the ground state and the excited states in an applied magnetic field. The value is inversely proportional to the energy differences ($\Delta E = E_e - E_g$) between the ground and excited states;[14] see eq 3. Thus for $\chi_{(TIP)}$ to be significant, ΔE must be small.

$$\chi_{(TIP)} = 2N\beta^2\sum\langle\psi_e|\hat{H}|\psi_g\rangle^2/\Delta E \qquad (3)$$

ψ_g and ψ_e are wave functions of the ground and excited states, respectively. In this case the orbitals of interest are the V^{4+} d orbitals. Therefore, if the $\chi_{(TIP)}$ and the orbital ordering in the ground state and excited states are known, ΔE can be calculated. In V_2O_5 xerogel, the vanadium is assumed to be in a distorted square-pyramidal geometry with approximate C_{2v} symmetry.[15] The idealized orbital diagram and d orbital splitting for C_{2v} symmetry are shown in Figure 8. On the basis of this scheme, the energy difference between the ground (electron in d_{xy} orbital) and excited (electron in d_{yz} or d_{xz} orbital) states is expected to be quite small. Therefore, eq 3 can be simplified into eq 4.[14a] The $\chi_{(TIP)}$ values

$$\chi_{(TIP)} = 4N\beta^2/\Delta E \qquad (4)$$

obtained are in emu/$A_xV_2O_5{\cdot}nH_2O$ which includes both V^{5+} and V^{4+} atoms. Based on the reasonable assumption that V^{5+} atoms make little or no contribution to the $\chi_{(TIP)}$[16], in order to calculate ΔE for the V^{4+} ions, $\chi_{(TIP)}$ must be normalized for the concentration of V^{4+}/V^{5+} in the V_2O_5 framework. The latter is known from the alkali ion loading. Using the *corrected* $\chi_{(TIP)}$ values in eq 4, the ΔE energies were calculated and are shown in Table 3. The ΔE values fall in the IR range, and remarkably, electronic absorptions in the same range are observed experimentally in the diffuse reflectance

(14) (a) Drago, R. S. *Physical Methods in Chemistry*; W. B. Sanders Co.: Philadelphia, 1977. (b) Boudreaux, X. A.; Mulay, L. N. *Theory and Applications of Molecular Paramagnetism;* John Wiley and Sons: New York, 1976.

(15) (a) Livage, J.; Gharbi, N.; Leroy, N. C.; Michaud, M. *Mater. Res. Bull.* **1978**, *13*, 1117−1124. (b) Stizza, S.; Davoli, I.; Benfatto, M. *J. Non-Cryst. Solids* **1987**, *95,96*, 327−334.

(16) TIP is expected in systems with low-lying vacant d-orbitals such as Mn^{7+}, Cr^{6+}, Ti^{4+}, and V^{5+} (Carrington, A. *Mol. Phys.* **1960**, *3*, 271). In the case of $V_2O_5{\cdot}nH_2O$ xerogel, the contribution of TIP from V^{5+} centers is negligible because magnetic susceptibility measurements follow a Curie−Weiss law without the need of any constant correction. Orthorhombic V_2O_5 has been reported to possess feeble paramagnetism (Raychaudhuri; Sengupta *Indian J. Phys.* **1936**, *10*, 245) but this relatively old work has not, to our knowledge, been confirmed in the recent literature.

Table 3. Corrected Temperature-Independent Paramagnetism and Calculated and Observed ΔE for $M_xV_2O_5{\cdot}nH_2O$ at Room Temperature

M	x	corrected $\chi_{(TIP)}$ (emu/mol)	$\Delta E_{(calcd)}$ (cm^{-1})	$\Delta E_{(obsd)}{}^a$ (cm^{-1})
K	0.08	1.4 ± 1.0e−3	2500	1900
K	0.26	8.5 ± 3.8e−4	2130	2800(w), 1500(s)
K	0.33	1.2 ± 0.3e−3	1100	1650
K	0.39	7.2 ± 2.0e−4	1920	1500
Cs	0.18	7.8 ± 4.4e−4	2940	2450
Cs	0.28	1.6 ± 0.4e−3	830	1650
Cs	0.35	1.0 ± 0.3e−3	1250	3000(w), 1590(s)
Cs	0.38	1.1 ± 0.3e−3	1270	1500

[a] Observed spectroscopically. w, weak; s, strong.

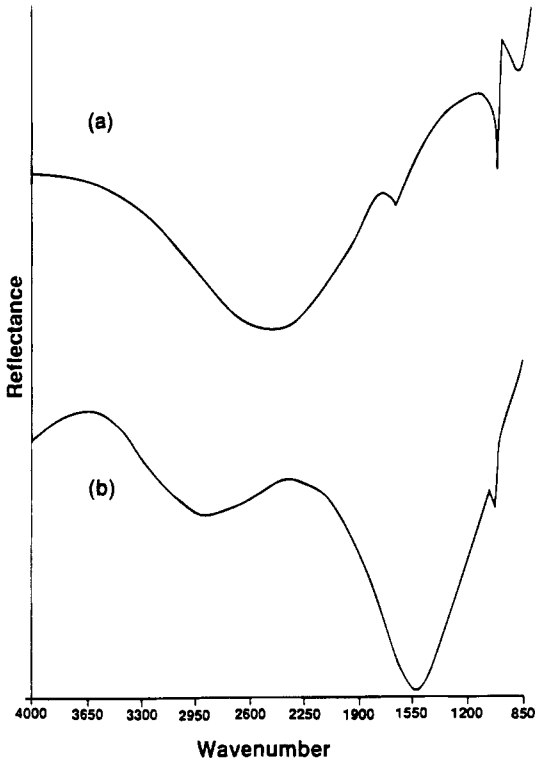

Figure 9. Diffuse reflectance IR spectra in the region where the electronic d → d transitions occur in (a) $K_{0.33}V_2O_5{\cdot}nH_2O$ and (b) $K_{0.47}V_2O_5{\cdot}nH_2O$. These bands are completely obscured when the spectra are taken in transmission using KBr pressed pellets.

IR spectra of the compounds; see Figure 9. The $A_xV_2O_5{\cdot}nH_2O$ materials show a strong broad band in the region 1500−2500 cm^{-1} (Table 3). Some compounds even have an additional band at ~3000 cm^{-1}, but it is considerably weaker. The bands are absent in the spectra of V_2O_5 xerogel. The average bandwidth of these transitions is considerably narrower (by a factor of 12) than the corresponding width of the intervalence charge-transfer transition centered at ~1400 nm. Furthermore, the intensity of the transitions in the region 1500−2500 cm^{-1} is significantly weaker than that of the intervalence transition and comparable to the strength of the vibrational transitions of the solid. These observations are consistent with the fact that these absorption bands are electronic d−d transitions associated with V^{4+} centers in a low-symmetry crystal field environment. In some phases two closely spaced transitions are observed, suggesting that the real electronic structure is much more complicated and possibly the existense of two kinds of V^{4+} ions with slightly different oxygen environments. Given that the uncertainty in the

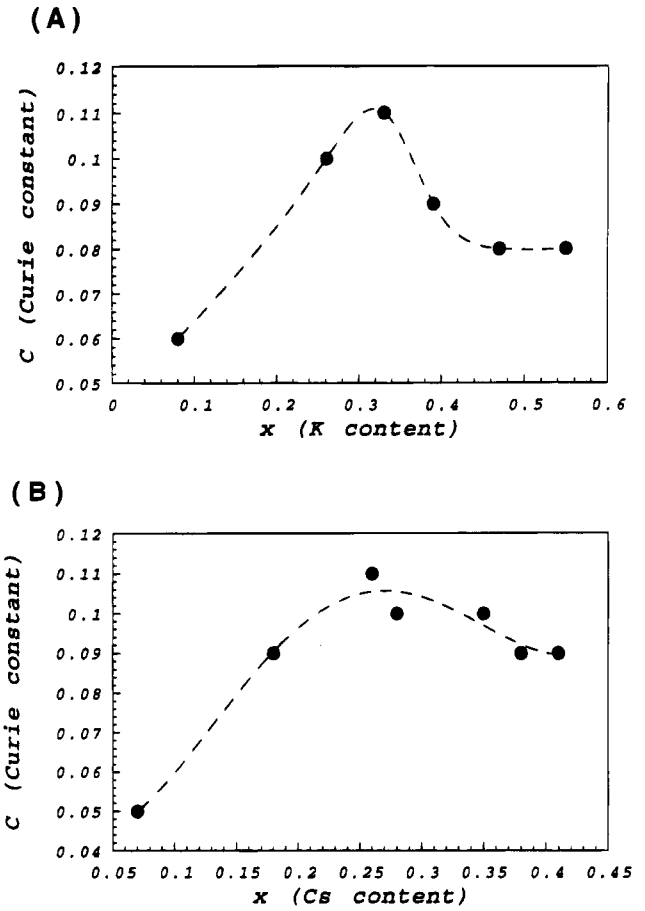

Figure 10. Plot of Curie constant, C, vs x (alkali content) for (a) $K_xV_2O_5{\cdot}nH_2O$ and (b) $Cs_xV_2O_5{\cdot}nH_2O$. The dotted lines through the data are used as guides to the eye and do not represent theoretical fits.

corrected $\chi_{(TIP)}$ values is large, the agreement between the calculated and spectroscopically observed values is satisfactory.

In $A_xV_2O_5{\cdot}nH_2O$, the Curie constant, C, is expected to increase linearly with the V^{4+} concentration. A linear relationship is indeed observed in the range $0 < x < 0.3$ but beyond $x \sim 0.3$ the Curie constant levels off and then declines somewhat at $x \sim 0.55$; see Figure 10. It is interesting to speculate on the decline of the magnetic susceptibility, beyond $x \sim 0.3$. In Oka's model, the closest V−V distance is 2.9 Å, involving dimers of vanadyl ions. As the number of spins introduced into the vanadium oxide framework is increased, the V=O/V=O dimers are populated by electrons. The loss of susceptibility may be due to strong antiferromagnetic coupling in these dimeric units. Such V=O/V=O dimers with V^{4+} centers are known in molecular species and can be antiferromagnetically coupled. Examples include $[(VO(DANA)]_2$[17] [DANA = 1,5-bis(*p*-methoxyphenyl)-1,3,5-pentanetrione] and $[V_2O_2Se_2(Se_2)_2]^{2-}$.[18] At low x values the d^1 centers are relatively isolated and give rise to Curie paramagnetism. As the number of these d^1 centers in the framework increases, it is reasonable to expect that the probability of d^1−d^1 dimer formation increases. Being antiferromagnetically coupled, the dimers will not contribute significantly to the suscep-

(17) Heeg, M. J.; Mack, J. L.; Glick, M. D.; Lintvedt, R. L. *Inorg. Chem.* **1981**, *20*, 833−839.
(18) Liao, J.-H.; Hill, L.; Kanatzidis, M. G. *Inorg. Chem.* **1993**, *32*, 4650−4652 and unpublished results.

tibility provided the coupling is $\gg kT$. This will lead to a leveling off or even a decrease of susceptibility with x at higher x values. Since this argument seems chemically plausible we decided to quantify it by modeling the magnetic behavior of the $Cs_xV_2O_5{\cdot}nH_2O$ system assuming the nearest neighbor coupling (d^1–d^1 dimer) is antiferromagnetic and large compared to kT. This is described in the next section.

Theoretical Considerations Concerning the Magnetic Susceptibility. In modeling the change in magnetic susceptibility for $A_xV_2O_5{\cdot}nH_2O$, we made the plausible assumption that the dominant interactions between d^1 centers is of Heisenberg type, with Hamiltonian

$$H = \sum J_{ij}\vec{S}_i{\cdot}\vec{S}_j \qquad (5)$$

where $\vec{S}_i$ is the spin at site i and J_{ij} is the interaction between sites. The observed behavior of the susceptibility χ, namely, the Curie–Weiss law with the Curie constant depending in a strong nonlinear manner on the concentration of spins (i.e., d^1 centers), *forces* one to conclude that some of the interactions are much larger than kT. This is so because if $J_{ij} \ll kT$ for all i,j, then it follows from eq 5 and equilibrium statistical mechanics that the susceptibility at such temperatures is Curie Weiss with C linear in x. Furthermore, if some of the J_{ij} were comparable to kT, then the characteristic T dependence observed would be violated. Hence we assume that some of the J_{ij} are $\gg kT$. Finally, the sublinear behavior of C with x suggests strongly that the large interactions are antiferromagnetic. Thus, we study models wherein the nearest-neighbor interactions are $\gg kT$, and antiferromagnetic, while further neighbor interactions are $\ll kT$. These assumptions lead to the Curie–Weiss law of eq 2, with θ linear in x and proportional to the further neighbor J_{ij}, and

$$C = C_1\sum_{n=0}^{\infty} w_{2n+1} \equiv C_1 W \qquad (6)$$

where $C_1 = g^2\beta^2/4k$ (the value for one isolated $S = {}^1/_2$ spin), and w_l is the number of isolated l clusters. An isolated l cluster is a cluster of l sites such that each site has at least one nearest neighbor in the cluster, and no site has a nearest-neighbor outside the cluster. The clusters with even l have a singlet ground state and therefore will not contribute to C.

Making the assumption that the V^{5+} are located randomly on the V sites, we have calculated C for the square and triangular 2-dimensional lattices and for a simple cubic 3-dimensional lattice, limiting the size of the clusters to keep the calculation tractable ($l = 5$ for the square and 3 for the triangular and simple cubic lattices).[19] W_N is the sum of W in (6) but taken only up to $2n + 1 = N$. In Figure 11 we show calculated curves, as a function of x,[20] for the square lattice. The convergence is seen to be good, the $l = 3$ result being a sufficiently good approximation. In Figure 12 the calculation for the triangular lattice is shown and compares well with the experimental data. Interestingly, the calculated result for the simple cubic lattice is quite similar to that of the triangular lattice but differs appreciably from that of the square lattice.

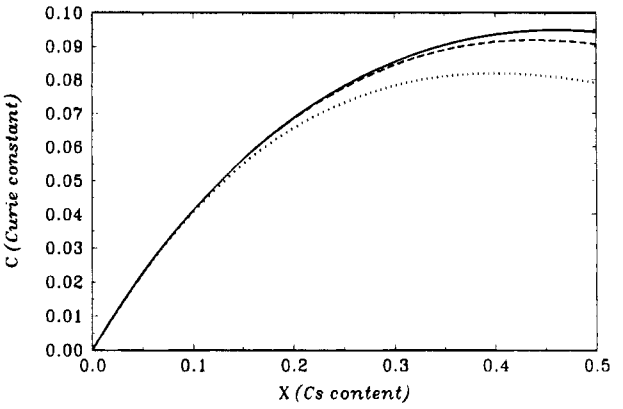

Figure 11. Curie constant, C (in units of C), as a function of V^{4+} concentration calculated for a square lattice. W_1, W_3, and W_5 are the dotted, dashed, and solid curves, respectively.

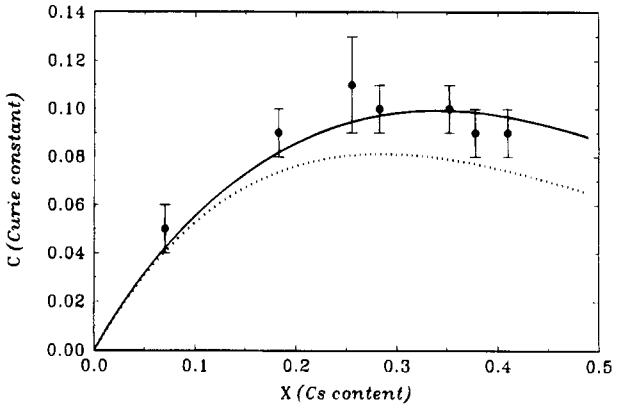

Figure 12. Curie constant, C, as a function of V^{4+} concentration calculated for a triangular lattice along with the experimental results. W_1 and W_3 are the dotted and solid curves, respectively. The theoretical result was multiplied by a scale factor to get the best fit.

The rather good agreement between the model for the triangular and simple cubic lattices and experiment is not meant to prove the correctness of the model. It is only meant to suggest that the basic ideas of the model, namely, that at the temperatures of interest some of the interactions are large (perhaps because of a local dimerization), and the remaining ones are small, compared to kT, give a possible explanation of the quite unusual behavior observed. Given the uncertainty in the structure of these materials, and the uncertainty of the J values even for a known structure, we feel that at present one cannot go much farther.

Electron Paramagnetic Resonance (EPR) Spectroscopy. The increased number of V^{4+} centers in the V_2O_5 framework of $A_xV_2O_5{\cdot}nH_2O$ is also reflected in the EPR spectra of these materials. The pristine V_2O_5 xerogel shows a hyperfine structure due to a small amount of V^{4+} ($I = {}^7/_2$) impurities in an axially distorted

(19) The calculation of the w_l is much more complicated for other lattices. In fact for these cases the highest l value we have obtained is 3. The problem is that for a given size cluster (given l), the number of clusters is of the form $y^l(1-y)^k$, where k depends on the topology or shape of the cluster. It is the enumeration of these various topologies that causes the complication. Fortunately, for the y values of interest, the sum is rather rapidly convergent.

(20) The definition of concentration x in the previous sections (as in $A_xV_2O_5{\cdot}nH_2O$) would give a concentration of $y = x/2$ spins per V site, provided there were no spins when $x = 0$. To take into account the residual spin at $x = 0$, discussed above, the appropriate value of y should be $y = (x + 0.04)/2$ (this assumes $g = 2$ and that $\mu_{eff} = 0.35\ \mu_B$ when $x = 0$).

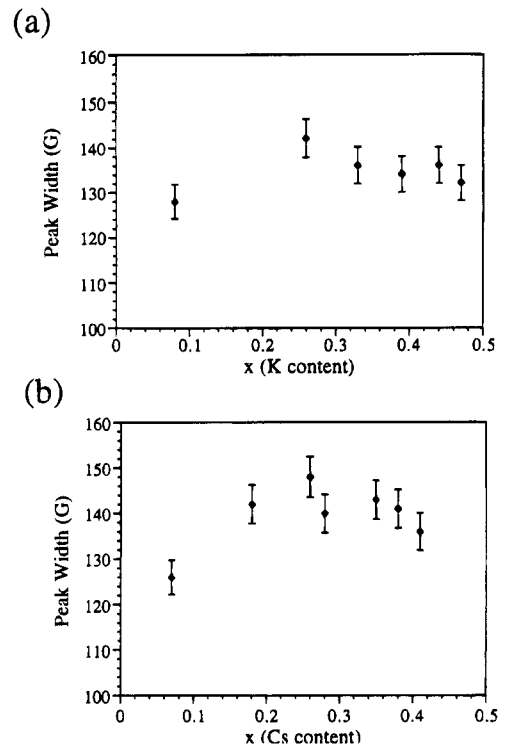

Figure 13. Changes of EPR peak width as a function of alkali ion loading for (a) $K_xV_2O_5{\cdot}nH_2O$ and (b) $Cs_xV_2O_5{\cdot}nH_2O$.

crystal field.[21] In $A_xV_2O_5{\cdot}nH_2O$, the increased V^{4+} centers enhance the spin–spin exchange reaction which converts the original hyperfine structure into a symmetric broad band with a g value centered at ca. 1.96. The peak width for all $A_xV_2O_5{\cdot}nH_2O$ materials varies as a function of x as illustrated in Figure 13. Interestingly, a maximum peak width is also observed at $x \sim 0.3$, consistent with the magnetic susceptibility data. This indicates that the spin density in the reduced framework is decreasing after $x > 0.3$ due to strong antiferromagnetic coupling, and it is consistent with the magnetic data discussed above.

Charge-Transport Measurements. Samples of $A_xV_2O_5{\cdot}nH_2O$ were studied in a pressed pellet form by dc electrical conductivity and thermopower measurements using the four-probe geometry. Compared with V_2O_5 xerogel, the $A_xV_2O_5{\cdot}nH_2O$ materials show at least a 1–2 orders of magnitude increase in electrical conductivity, to 10^{-3}–10^{-2} S/cm at room temperature. No evidence of ionic contributions to the conductivity was observed. Generally, the conductivity slightly increases with the x as shown in Figure 14, consistent with a small polaron conductor where charge transport is due to electron hopping. Thus, conductivity increases with the number of charge carriers (V^{4+}) in the framework but levels off at $x > 0.42$. The conductivity measurements on granular samples alone do not unequivocally characterize their electrical behavior. A complementary probe to address this issue is thermoelectric power (TP) measurements as a function of temperature. TP measurements are typically far less susceptible to artifacts arising from the resistive domain boundaries in the material because they are essentially zero-current measurements. This is because the temperature drop across such boundaries is much less significant than the voltage drop. Figure 15 shows typical TP data for $K_xV_2O_5{\cdot}nH_2O$ as a function of temperature. Accurate measurements at low temperature were hindered by the very large sample resistances that developed. The Seebeck coefficients for these materials are negative with relatively large absolute values confirming a n-type semiconductor. The rate of increase in Seebeck coefficient slows with increasing x, resulting in a leveling off at ~ -30 μV/K

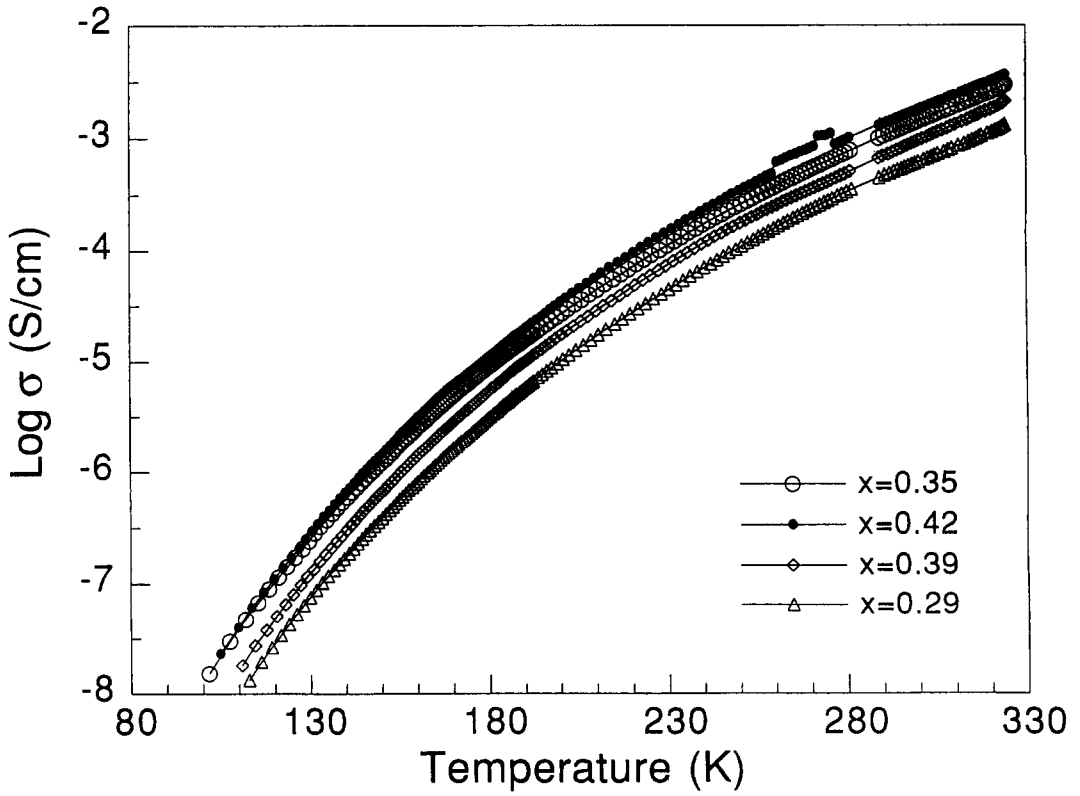

Figure 14. Four-probe pressed-pellet variable-temperature electrical conductivity data of $K_xV_2O_5{\cdot}nH_2O$.

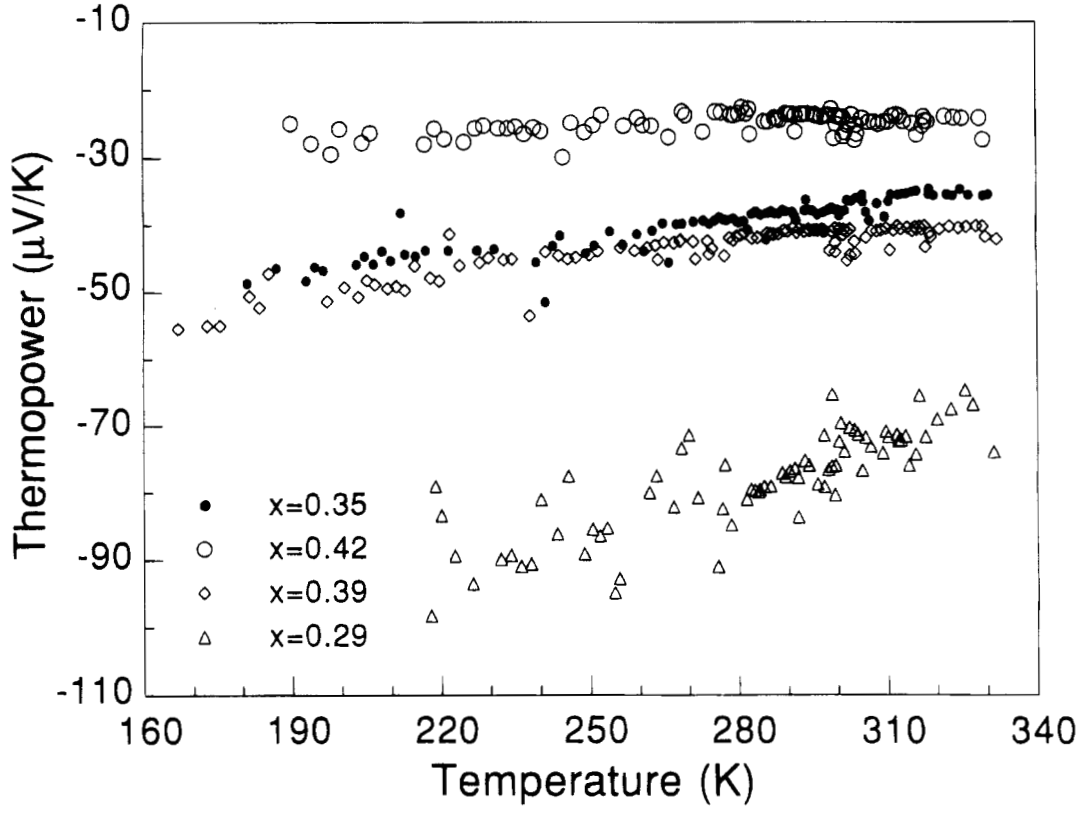

Figure 15. Variable-temperature thermoelectric power data of $K_xV_2O_5{\cdot}nH_2O$.

at $x > 0.35$, consistent with the increasing number of charge carriers in the range of $0 < x < 0.35$ followed by a leveling off afterward. The conductivity values observed in the entire family of $A_xV_2O_5{\cdot}nH_2O$ do not exceed 10^{-2} S/cm at room temperature, which probably represents an approximate upper bound for these kinds of materials. The charge transport in $A_xV_2O_5{\cdot}nH_2O$ is exclusively due to the reduced vanadium oxide framework and any possible enhancements observed beyond the levels reported here in redox intercalation compounds of $V_2O_5{\cdot}nH_2O$ (e.g., conjugated polymers[1]) must be attributed to the intercalating species.

Concluding Remarks

The use of bronze-like $A_xV_2O_5{\cdot}nH_2O$ phases has allowed the studies of the reduced V_2O_5 xerogel framework without interference from the intercalants. The optical and magnetic properties of these phases are intriguing and associated with the environments and interactions of V^{4+} atoms in the V_2O_5 framework. These phases show relatively low-energy d–d electronic transitions occurring in the infrared range and a small but significant temperature-independent paramagnetism. Similar phenomena were also observed in all polymer/V_2O_5 intercalation compounds.[22] These studies indicate that the origin of these phenomena is the reduced V_2O_5 framework and not the interactions between the polymers and the framework. Interestingly, these $A_xV_2O_5{\cdot}nH_2O$ phases show a maximal spin density and Curie constant at $x \sim 0.3$ consistent with strong antiferromagnetic coupling ($\gg kT$) between neighboring spins beyond this value of x. Although such antiferromagnetic coupling is usual among d^1 systems, the unusual magnetic behavior outlined in this paper has not been observed before in a similar series of homologous compounds.

Acknowledgment. Financial Support from the National Science Foundation (DMR-93-06385) is gratefully acknowledged. This work made use of the SEM facilities of the Center for Electron Optics at Michigan State University. At NU this work made use of Central Facilities supported by NSF through the Materials Research Center (DMR-91-20521). We thank Professor S. D. Mahanti for fruitful discussions and C. N. Hoff for some of the magnetic susceptibility calculations.

CM950032Z

(21) (a) Sanchez, C.; Babonneau, F.; Morineau, R.; Livage, J.; Bullot, J. *Philos. Mag. B* **1983**, *3*, 279. (b) Barboux, P.; Gourier, D.; Livage, J. *Colloids Surf.* **1984**, *11*, 119.

(22) (a) Wu, C.-G. Ph.D. Dissertation; Michigan State University, 1992. (b) Liu, Y.-J.; DeGroot, D. C.; Schindler, J. L.; Kannewurf, C. R.; Kanatzidis, M. G. *Adv. Mater.* **1993**, *5(5)*, 369–372.